Nuclear absorption effects in the elastic scattering of ^{10}B and ^{11}B by ^{27}Al, ^{28}Si, and ^{30}Si

L. A. Parks,* K. W. Kemper, R. I. Cutler, and L. H. Harwood†
Department of Physics, Florida State University, Tallahassee, Florida 32306
(Received 16 January 1979)

Elastic scattering angular distributions for ^{10,11}B + ^{27}Al, ^{28,30}Si at E_{lab} = 41.6 and 50 MeV, ^{10,11}B + ^{28}Si at E_{lab} = 33.7 MeV, and ^{11}B + ^{28}Si at E_{lab} = 41.1 and 42.1 MeV have been measured. At each energy all angular distributions show similar oscillatory structure for $\sigma/\sigma_R > 10^{-3}$, except for ^{11}B + ^{28}Si, which is comparatively structureless. The inelastic scattering angular distributions of the first excited 2^+ states in ^{28}Si by ^{10,11}B at E_{lab} = 33.7, 41.6, and 50 MeV, and in ^{30}Si by ^{10,11}B at 50 MeV and by ^{10}B at 41.6 MeV are presented. Relative direct transfer reaction strengths for ^{11}B + ^{27}Al and ^{11}B + ^{28}Si were measured at 49.5 MeV. The differences in the measured elastic scattering angular distributions can be explained by stronger direct transfer reaction channels in ^{11}B + ^{28}Si.

[NUCLEAR REACTIONS: ^{27}Al(^{10,11}B, ^{10,11}B)^{27}Al, E=41.6 and 50 MeV; ^{28,30}Si(^{10,11}B, ^{10,11}B)^{28,30}Si, elastic and Si inelastic (^{28}Si, 2^+, 1.78 MeV; ^{30}Si, 2^+, 2.23 MeV), E=33.7, 41.6, and 50 MeV. Measured $\sigma(\theta)$, deduced optical model parameters and Si 2^+ deformation lengths. Measured particle transfer cross sections, ^{11}B+^{27}Al, ^{28}Si E=49.5 MeV, θ_L=14.7°, 18°, and 21°.]

I. INTRODUCTION

Many surprising and interesting phenomena have recently been observed in heavy-ion elastic scattering. One of these effects was observed in the study of 50 MeV ^{10,11}B elastic scattering by ^{27}Al done by Parks *et al.*[1] It was found that the forward angle oscillations in the angular distributions became damped in the angular range of $50° \lesssim \theta_{c.m.} \lesssim 80°$. This damping was attributed to the influence of the quadrupole deformations of the ^{10,11}B projectiles. The differences in the scattering of the boron projectiles prompted a more detailed study of the scattering from other targets with masses close to 27. In the present work, the results of a study of the scattering of ^{10}B and ^{11}B by ^{27}Al, ^{28}Si, and ^{30}Si at the bombarding energies of 34, 42, and 50 MeV are presented. Additionally, ^{11}B elastic scattering by ^{28}Si was measured at 41.1 and 42.1 MeV to search for any rapid changes in structure of the angular distributions.

Because of the forward angle elastic scattering differences observed in the systems studied in the present work, the ^{11}B + ^{27}Al, ^{28}Si transfer reaction cross sections were measured at three angles around $\sigma_{elastic}/\sigma_{Ruth}$=0.25, and these results are presented. Also presented are data and distorted-wave Born approximation (DWBA) calculations for the inelastic scattering of ^{10}B and ^{11}B by ^{28}Si and ^{30}Si.

II. EXPERIMENTAL APPARATUS AND TECHNIQUES

The ^{10,11}B beams were obtained from an inverted sputter source[2] and accelerated by the Florida State University Super FN Tandem Van de Graaff Accelerator to energies from 33.7 to 50 MeV. Target currents were 5 to 500 namp (electrical). The smaller target currents were used at the far forward angles so as to minimize dead time.

The Al targets for the elastic scattering studies were 50 μg/cm^2, 100 μg/cm^2, and 200 μg/cm^2 thick and self-supporting. The $^{28,30}SiO_2$ targets were 110 μg/cm^2 and 220 μg/cm^2 thick and self-supporting. The ^{28}Si and ^{30}Si targets were isotopically pure to 99.84% and 95.55%, respectively. When either the 200 μg/cm^2 ^{27}Al or 220 μg/cm^2 $^{28,30}SiO_2$ targets were used, the beam energy was increased by 100 keV to compensate for additional energy losses in the thicker targets.

The elastic scattering data were taken in a 46 cm diameter scattering chamber with an array of 300 μm and 100 μm thick silicon surface barrier detectors separated by 10°. The detector angular acceptances ranged from 0.25° for the forward angle detectors to 1.0° for the far back angle detectors. Most data were taken in 1° steps to ensure that no fine angular structure would be missed. Several angles were repeated by at least 2 detectors as a check for consistency. Data for angles >50° were taken with solid state E-ΔE counter telescopes to minimize the background from α particles and other reaction products. A monitor detector was used to note possible charge collection errors and target thickness variations from run to run.

For each of the cases studied, relative cross sections, corrected for dead time (≤5% for all angles), were first determined. To arrive at absolute cross sections, the product of the target

thickness and the solid angle ($N_T d\Omega$) was determined by scattering 6 MeV α particles by ^{27}Al, ^{28}Si, and ^{30}Si at 4 to 6 angles within the angular range of 16° to 26°. Small beam defining collimators were placed about 2.5 cm in front of the targets to eliminate any inaccuracies due to target nonuniformity. These measurements indicated that α-particle scattering is Rutherford within this angular range. ^{10,11}B scattering at the energies of interest was then performed on the same targets in the same geometry, and several angles common to the previously obtained relative angular distributions were measured.

All of the data illustrated in this study will show the statistical errors represented by error bars, unless the error bars are smaller than the size of the data points. The angle setting uncertainty was measured to be ±0.1°. The effect of this error is most important at the far forward angles and is included in the error bars of the elastic scattering angular distributions plotted as σ/σ_R vs $\theta_{c.m.}$, where σ_R is the Rutherford cross section. The absolute uncertainty of both the elastic and the inelastic scattering cross sections is ±6%.

The ^{11}B + ^{27}Al, ^{28}Si reaction data were measured at 49.5 MeV (lab) in an 80 cm diameter scattering chamber with an E-ΔE counter telescope at lab angles of 14.7°, 18.0°, and 21.0°. A 15 μm solid state transmission detector was used as the ΔE detector, and a 300 μm silicon surface barrier detector was used as the E detector. The telescope was cooled to −20 °C to improve the total energy resolution. These measurements involved the observation of $_3$Li through $_9$F reaction products.

For the reaction measurements, the Al targets were 20 μg/cm^2 thick, evaporated onto thin Formvar backings. These targets were kept under vacuum after fabrication to minimize the buildup of oxygen and hydrogen on the surfaces.

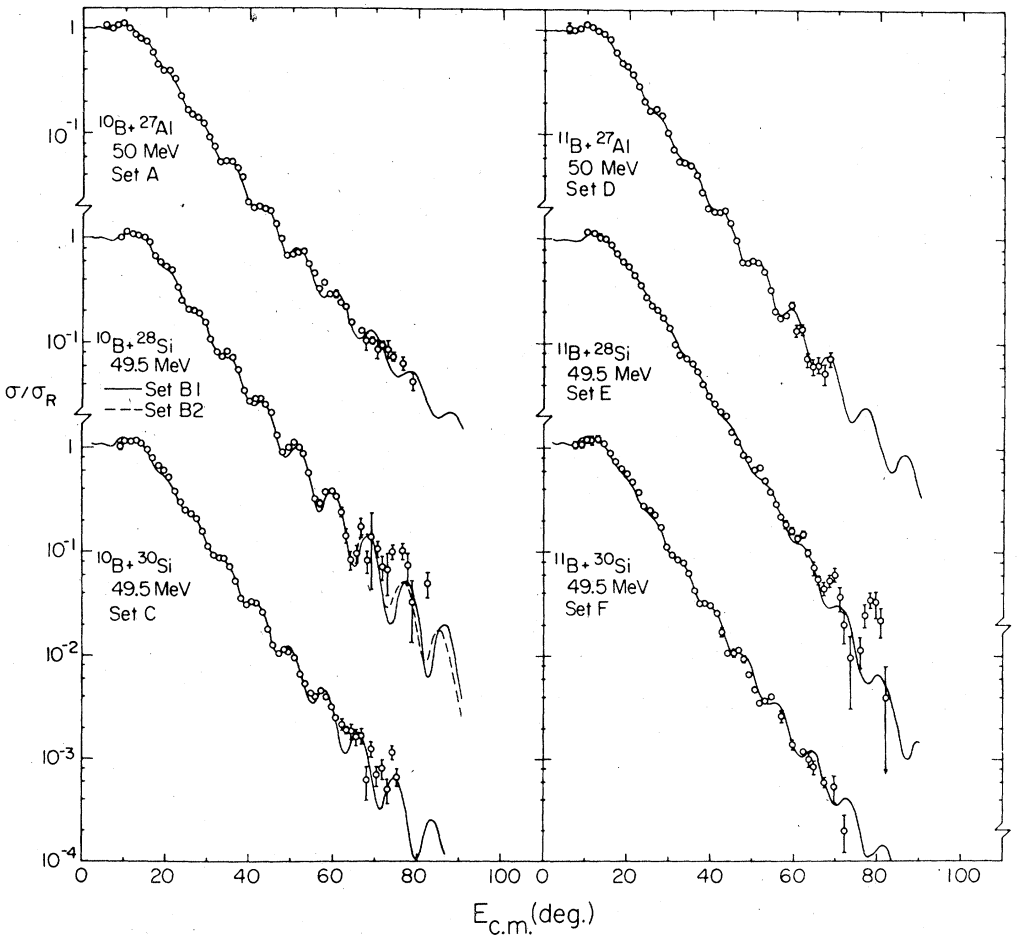

FIG. 1. Ratio of the elastic cross section to the Rutherford cross section for ^{10,11}B+^{27}Al, ^{28,30}Si at E_{lab}= 50 MeV. See the text for discussions of the optical model calculations and errors. The potential sets for the optical model calculations are listed in Table I.

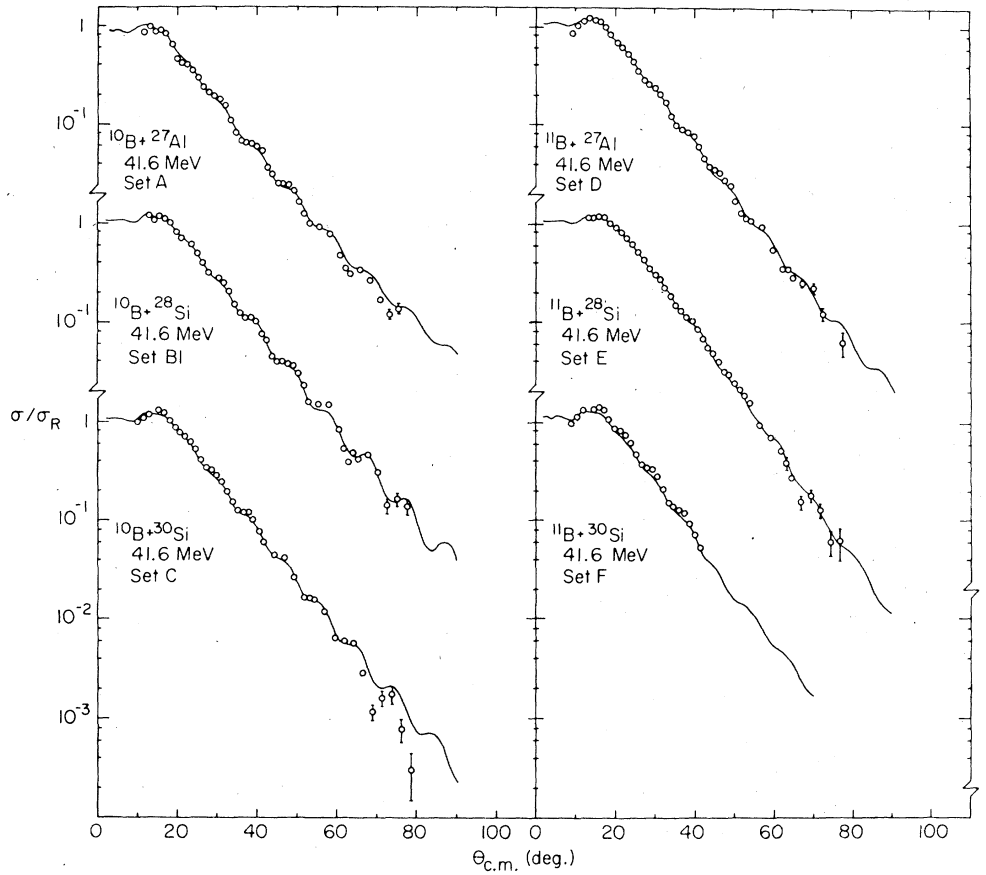

FIG. 2. Same as Fig. 1, except $E_{1ab}=41.6$ MeV.

Isotopically pure 110 $\mu g/cm^2$ thick $^{28}SiO_2$ targets, previously discussed, were used to observe the ^{28}Si reaction products. To correct for the oxygen content of this target, corresponding data were also taken on targets of 20 $\mu g/cm^2$ $^{27}Al_2O_3$ evaporated onto thin Formvar backings. Additionally, data were taken on thin Formvar targets to correct for unwanted contributions from the Formvar backings in the ^{27}Al and $^{27}Al_2O_3$ runs. The contribution due to the oxygen in the $^{28}SiO_2$

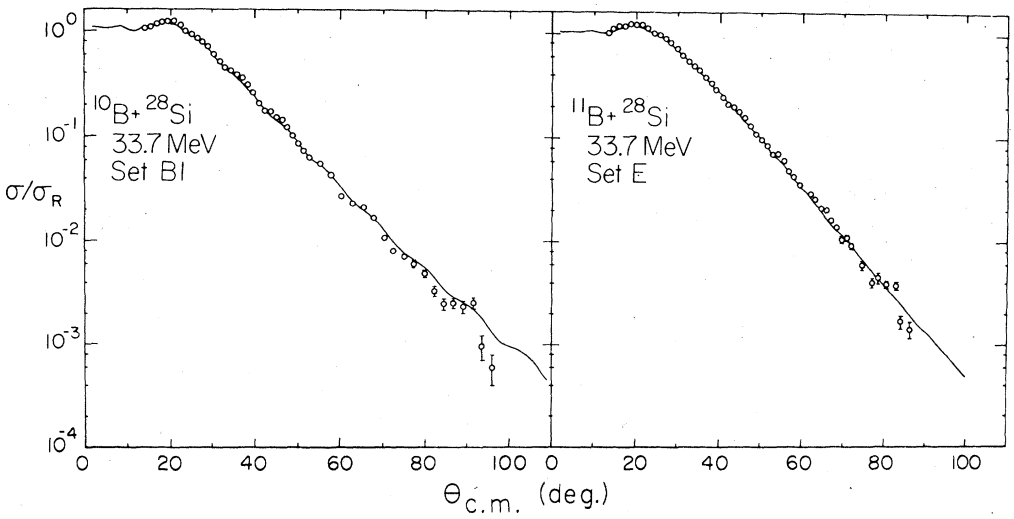

FIG. 3. Same as Fig. 1, except only $^{10,11}B+^{28}Si$ at 33.7 MeV are shown.

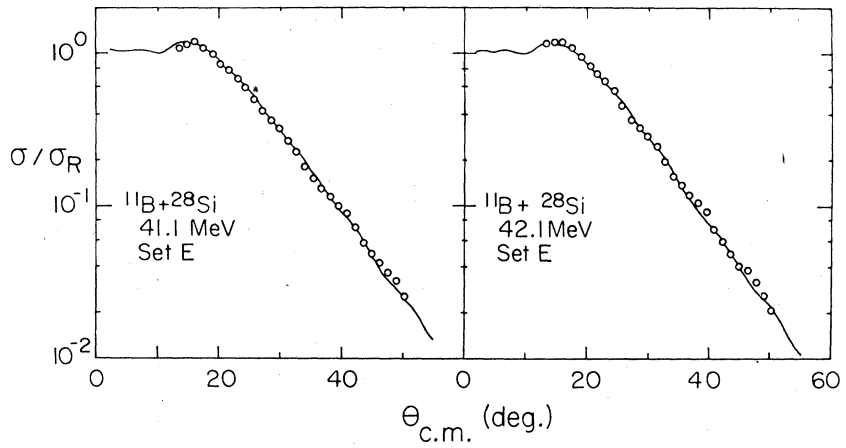

FIG. 4. σ/σ_R for $^{11}B+^{28}Si$ at $E_{lab}=41.1$ and 42.1 MeV. The optical model calculations shown used potential set *E*, listed in Table I.

target was subtracted by using the normalized oxygen yields obtained from the ^{11}B induced reactions on the ^{27}Al, $^{27}Al_2O_3$, and Formvar targets.

III. ANALYSIS AND RESULTS

A. Elastic scattering

The angular distributions obtained from the elastic scattering of $^{10,11}B+^{27}Al$, $^{28,30}Si$ taken at 50 and 41.6 MeV and of $^{10,11}B+^{28}Si$ at 33.7 MeV are shown in Figs. 1–3. At each energy, except for $^{11}B+^{28}Si$, all of the angular distributions are similar in structure and exhibit regular diffraction oscillations, beginning at $\sigma/\sigma_R \approx 10^{-1}$, which become more pronounced at the higher energies. The angular distributions for $^{11}B+^{28}Si$ do not show these oscillations, but do show strong oscillations beginning at $\sigma/\sigma_R \approx 10^{-3}$. Figure 4 shows $^{11}B+^{28}Si$ elastic scattering angular distributions taken at 41.1 and 42.1 MeV. These measurements exhibit the same structureless angular distributions seen at 33.7, 41.6, and 49.5 MeV.

The curves in Figs. 1–4 show the results of optical model calculations obtained by using the computer code JIB.[3] The optical model parameters for these curves and the form of the potential used are listed in Table I. These parameters were obtained by first searching upon the real and imaginary well depths, U and W, to obtain the best fit to the data for a set of diffusenesses, $a_R=a_I=0.60$ to 0.86 fm in 0.02 fm steps. The real and imaginary radius parameters were $r_0=1.05$ fm, and the Coulomb radius parameter was $r_C=1.34$ fm. Next, a_r and a_I were uncoupled and individually varied about their previously optimized value, while searching on U and W to obtain a better fit to the data. The 50 MeV data were fitted first, and the best parameter set for each target-projectile combination was used as a starting point to fit the lower energy data. Only the parameters U and W were varied to fit the lower energy data. The 50 MeV ^{10}B data were only fitted for $\sigma/\sigma_R \gtrsim 10^{-2}$ to avoid complications at back angles from possible contributions from the ^{10}B quadrupole deformation.[1,4] The 50 MeV $^{11}B+^{28}Si$ were fitted for $\sigma/\sigma_R \gtrsim 10^{-3}$, since pro-

TABLE I. Derived optical model potentials.

$$V(r)=\frac{-U}{1+\exp(r-R_R)/a_R}-\frac{iW}{1+\exp(r-R_I)/a_I}+V_C(r)$$

$$R_i=r_i(A_p^{1/3}+A_T^{1/3}) \quad (i=R,I,C).$$

System	Set	U (MeV)	r_R (fm)	a_R (fm)	W (MeV)	r_I (fm)	a_I (fm)	r_{Coul} (fm)
$^{10}B+^{27}Al$	*A*	38.7	1.05	0.85	99.0	1.05	0.62	1.34
$^{10}B+^{28}Si$	*B*1	85.7	1.05	0.69	91.6	1.05	0.62	1.34
	*B*2	14.2	1.34	0.60	11.3	1.34	0.60	1.34
$^{10}B+^{30}Si$	*C*	82.6	1.05	0.69	96.9	1.05	0.62	1.34
$^{11}B+^{27}Al$	*D*	41.7	1.05	0.79	66.1	1.05	0.66	1.34
$^{11}B+^{28}Si$	*E*	36.5	1.05	0.74	29.8	1.05	0.81	1.34
$^{11}B+^{30}Si$	*F*	47.8	1.05	0.79	79.0	1.05	0.66	1.34

nounced oscillations are forming at larger angles. The final parameters listed in Table I were obtained by taking the average of the real and imaginary well depths for each system at all energies. These averaged parameters reproduce the data nearly as well as the optimum individual parameter sets. The parameters obtained for $^{10}B + ^{27}Al$, $^{10}B + ^{30}Si$, and $^{11}B + ^{28}Si$ exhibit negligible energy dependence. For $^{10}B + ^{28}Si$, $^{11}B + ^{27}Al$, and $^{11}B + ^{30}Si$, the energy dependence is dU/dE, $dW/dE < 2$.

One other potential set for $^{10}B + ^{28}Si$ is listed in Table I and the resulting optical model calculation is also shown in Fig. 1. This set, designated $B2$, fits the data as well as the set with $r_0 = 1.05$ fm, designated $B1$. Set $B2$ was obtained in the same manner as the procedure discussed above, except the radius parameters were initially set to $r_0 = 1.34$ fm. These larger radius parameters necessitated very shallow potential wells compared to those where $r_0 = 1.05$ fm. Sets $B1$ and $B2$ will be discussed in more detail in the discussion of the inelastic scattering analysis.

All of the potential sets listed in Table I exhibit continuous Igo ambiguities.[5] As a consequence of the Igo ambiguity, reasonable radius parameters may be specified, and diffuseness parameters and well depths can be found which adequately reproduce the data. This is the justification of not initially searching upon radius parameters.

Heavy-ion elastic scattering inspects only the tail region of the nuclear potential,[6,7] principally due to the strongly absorptive nature of heavy-ion interactions above the Coulomb barrier. Perhaps the only physical information which may be obtained from heavy-ion elastic scattering is the determination of the strong absorption radius and the value of the real nuclear potential at this point.[7] These values were obtained by varying the optimum a_R by ±0.02 fm and searching on the real potential well depth to arrive at an acceptable fit to the data. The intersection point of the three potentials was taken to be the strong absorption radius. The strong absorption radii and corresponding real potentials are listed in Table II for all target-projectile systems and all energies in this study. For $^{11}B + ^{28}Si$, the real potential is weaker than for the other systems while the absorption is the same so that the ratio W/U implies more absorption for $^{11}B + ^{28}Si$ than for other systems. It should be emphasized that all of the data could not be reproduced by a single potential set, showing that it was not possible to obtain a universal heavy-ion potential for the different systems.[8] The deviations of the data from the calculated elastic cross sections at larger angles ($\sigma/\sigma_R \leq 10^{-3}$) are of the correct magnitude to be consistent with contributions from the quadrupole moments of ^{10}B and ^{11}B.[1,4] A more detailed analysis of the quadrupole contributions to the elastic scattering is currently in progress.

TABLE II. Tabulation of strong absorption radii, $r_{s.a.}$, real potentials $U(r_{s.a.})$, and ratios of $W(r_{s.a.})/U(r_{s.a.})$ evaluated at the strong absorption radii for $^{10,11}B + ^{27}Al$, $^{28,30}Si$.

System	E_{lab} (MeV)	$r_{s.a.}$ (fm)	$U(r_{s.a.})$ (MeV)	$W(r_{s.a.})/U(r_{s.a.})$
$^{10}B + ^{27}Al$	50	7.7	2.4	0.98
	41.6	8.3	1.3	0.74
$^{10}B + ^{28}Si$	49.5	8.4	1.2	0.66
	41.6	8.6	0.88	0.64
	33.7	9.0	0.50	0.60
$^{10}B + ^{30}Si$	49.5	8.7	0.82	0.70
	41.6	8.8	0.71	0.68
$^{11}B + ^{27}Al$	50	8.2	1.3	0.82
	41.6	8.7	0.70	0.72
$^{11}B + ^{28}Si$	49.5	8.7	0.49	1.18
	41.6	8.8	0.43	1.19
	33.7	8.8	0.43	1.19
$^{11}B + ^{30}Si$	49.5	8.6	1.0	0.79
	41.6	8.8	0.82	0.75

B. Inelastic scattering

The inelastic scattering angular distributions for $^{28}Si(^{10,11}B, ^{10,11}B)^{28}Si^*$ at 49.5, 41.6, and 33.7 MeV, $^{30}Si(^{10}B, ^{10}B)^{30}Si^*$ at 49.5 and 41.6 MeV, and $^{30}Si(^{11}B, ^{11}B)^{30}Si^*$ at 49.5 MeV are shown in Figs. 5–7. It was not possible to make measurements for angles less than $\theta_{c.m.} \approx 30°$ because of the large oxygen elastic peak from the $^{28,30}SiO_2$ targets. For $^{11}B + ^{28}Si$, where the inelastic ^{28}Si and ^{11}B peaks are well separated, projectile excitation was observed to be weak. It was therefore assumed that the inelastic scattering angular distributions correspond to the excitation of the rotational first-excited 2^+ states in ^{28}Si (1.78 MeV) and ^{30}Si (2.23 MeV), and not that of an excited state of the projectile, ^{10}B or ^{11}B.

Inelastic scattering calculations using the zero range DWBA code DWUCK[9] with a collective form factor for the nuclear excitation are also shown in Figs. 5–7. The calculations were done with a $\Delta l = 2$ transfer using the optical model parameters obtained from the elastic scattering analysis. Eighty partial waves were used and the integration was performed in step intervals of 0.08 fm from 0.0 to 30 fm. The results are the same when 90 partial waves are used and the integration is performed in step intervals of 0.1 fm from 0.0 to 40 fm. Coulomb excitation was found to be unimportant at 49.5 and 41.6 MeV over the angular range of interest ($\theta_{c.m.} \gtrsim 35°$), but was included at 33.7 MeV. For the latter energy, 149 partial

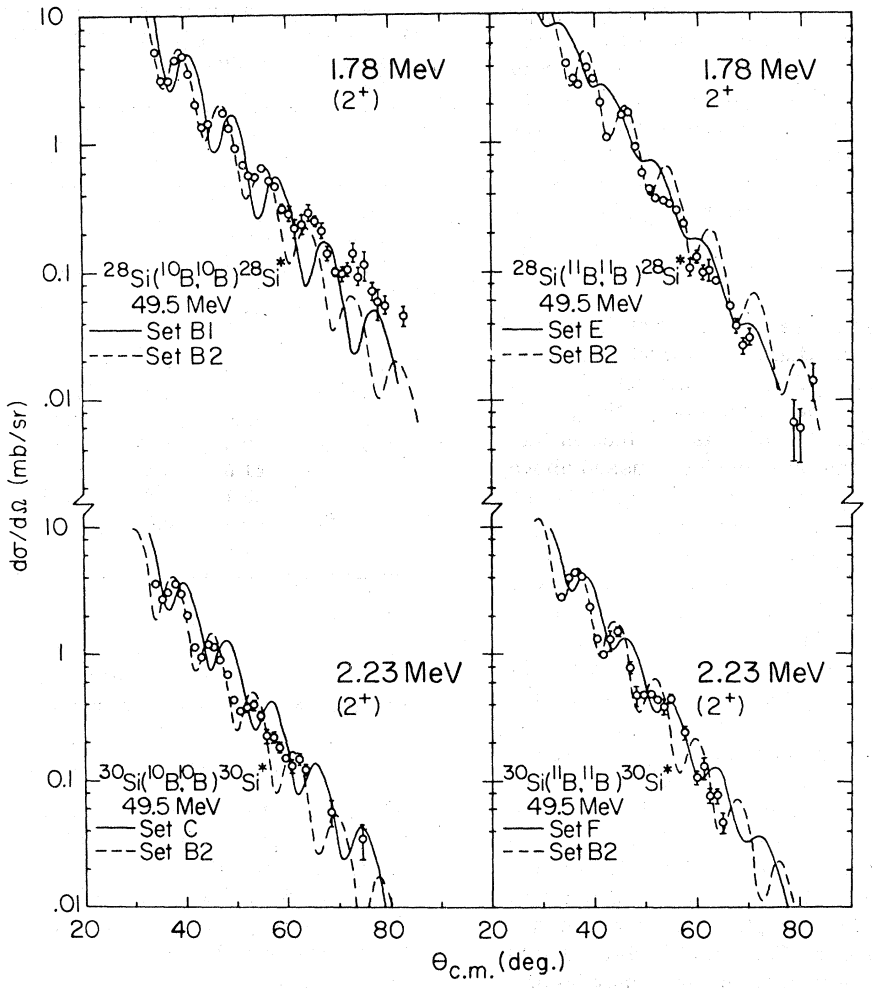

FIG. 5. Angular distributions for the inelastic excitation of the first-excited 2^+ states in ^{28}Si (1.78 MeV) and ^{30}Si (2.23 MeV) by ^{10,11}B at 49.5 MeV. It is assumed that there is negligible excitation of the ^{10,11}B at the same excitation energies as the Si 2^+ states. The solid curves are DWBA calculations using a collective form factor and potential sets in Table I. Coulomb excitation is not included.

waves were used and the integration was performed in 0.1 fm steps from 0.0 to 39.9 fm.

The calculations using the optical model parameters with $r_0 = 1.05$ fm are about 2° out of phase with the data at 49.5 and 41.6 MeV. This phase problem is not as apparent at 33.7 MeV. However, the calculation using potential set $B2$ ($r_0 = 1.34$ fm) is in phase with the ^{28}Si(^{10}B, ^{10}B)^{28}Si* data. This is an example of two optical model potential sets which reproduce the elastic scattering data equally well, but differ in their fit to the inelastic scattering data. Potential set $B2$ was also used to generate calculations for the other systems at 49.5 MeV. In each case, the calculations are in phase with the data. The inelastic scattering analysis is consistent with the energy independent potential found for ^{16}O + ^{28}Si by Cramer *et al.*[8]

The deformation parameters β_N obtained for the 49.5 MeV scattering measurements are listed in Table III. Also listed in Table III are the corresponding quadrupole deformation lengths δ_2, where

$$\delta_2 = \beta_N r_0 A_T^{1/3}.$$

These are compared with previously measured deformation lengths, also listed in Table III. The deformation lengths determined in this study are somewhat smaller than previously determined values.

The significant point of this study is that direct comparisons of ^{28}Si(^{10}B, ^{10}B)^{28}Si* with ^{28}Si(^{11}B, ^{11}B)^{28}Si* and ^{30}Si(^{10}B, ^{10}B)^{30}Si* with ^{30}Si(^{11}B, ^{11}B)^{30}Si* at the energies presented show that the angular distributions are similar in both magnitude and structure. In particular, both the ^{28}Si(^{10}B, ^{10}B)^{28}Si* and ^{28}Si(^{11}B, ^{11}B)^{28}Si* inelastic

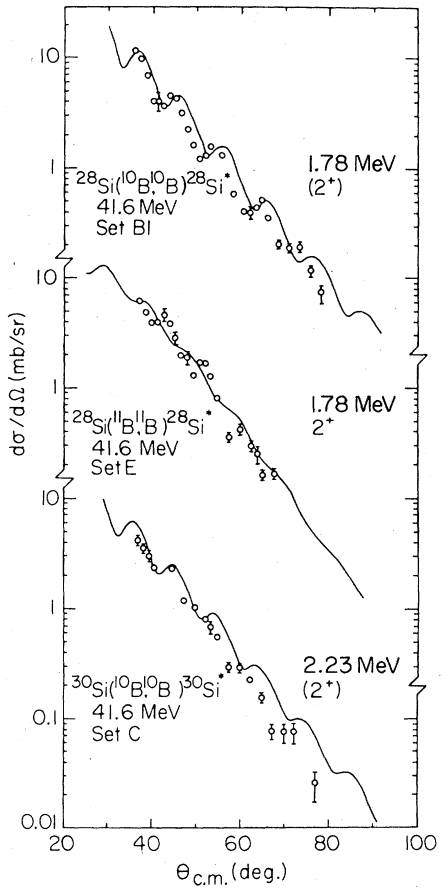

FIG. 6. Same as Fig. 8, except the inelastic scattering angular distributions are shown for ^{10,11}B+^{28}Si and ^{10}B+^{30}Si at 41.6 MeV.

scattering angular distribution exhibit oscillations, while only the elastic scattering of ^{10}B+^{28}Si shows oscillations in the angular distributions. Also, there is no significant enhancement for ^{11}B inelastic scattering compared to ^{10}B scattering.

C. ^{11}B+^{27}Al, ^{28}Si reaction analysis

As discussed previously, the ^{11}B+^{27}Al and ^{11}B+^{28}Si elastic scattering angular distributions at 50 MeV are dissimilar about their grazing angles, indicating a major difference in the two systems for the grazing partial waves. The optical model analysis of the elastic scattering data shows that there is stronger absorption for ^{11}B+^{28}Si than for ^{11}B+^{27}Al (see Table II) at the strong absorption radius, so enhanced direct reaction cross sections are expected for ^{11}B+^{28}Si relative to those for ^{11}B+^{27}Al. From the elastic data, the grazing angles (where $\sigma/\sigma_R \approx 0.25$) for ^{11}B+^{27}Al, ^{28}Si at 50 MeV are at $\theta_{lab} \approx 18°$. Since few nucleon transfer reactions are the major contributors to the absorbed strength for grazing partial waves,[10] a comparison of transfer reaction strengths at the grazing angle may explain the elastic scattering differences.

Figure 8 shows multiparameter E-ΔE spectra of 49.5 MeV ^{11}B+^{28}SiO$_2$ taken at $\theta_{lab} = 18°$. Two ΔE amplifier gains were used so that good Z resolution could be attained for all $Z \geq 3$ reaction products. Individual particle groups could be resolved from ^{6}Li through ^{12}C. The particle spectra from $^{6}_{3}$Li through $^{12}_{6}$C were generated by drawing two-dimensional gates around the multiparameter particle groups. The N, O, and F Z groups were

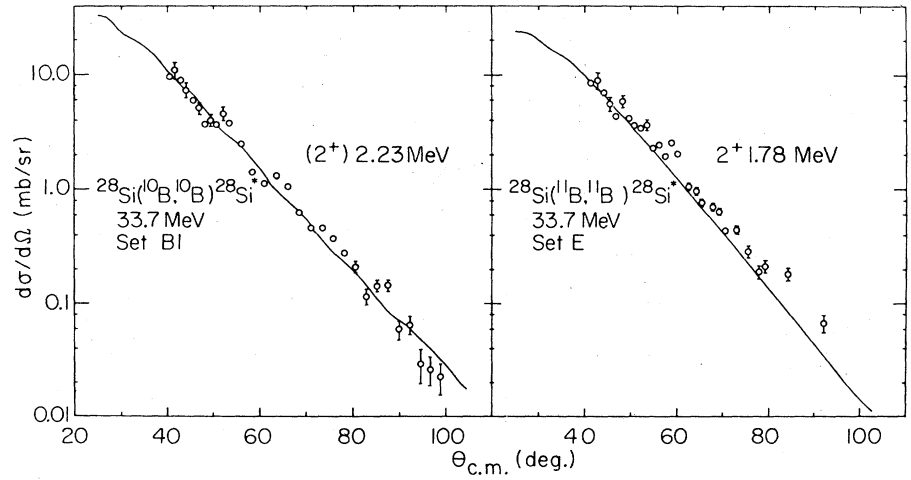

FIG. 7. Same as Fig. 8, except the inelastic scattering angular distributions are shown for ^{10,11}B+^{28}Si at 33.7 MeV. Coulomb excitation is included.

TABLE III. Quadrupole deformation parameters and deformation lengths for the 2^+ states in ^{28,30}Si populated by the inelastic scattering of 49.5 MeV ^{10,11}B.

System	Potential set	Present study β_N	Present study δ_2 (fm)	Previous studies δ_2 (fm)
^{10}B+^{28}Si	*B*1	0.36	1.15	1.32±0.19 [a]
	*B*2	0.24	0.99	
^{11}B+^{28}Si	*E*	0.34	1.07	
	*B*2	0.21	0.84	
^{10}B+^{30}Si	*C*	0.29	0.94	1.05 [b]
	*B*2	0.19	0.81	
^{11}B+^{30}Si	*F*	0.32	1.03	
	*B*2	0.19	0.78	

[a] W. J. Thompson and J. S. Eck, Phys. Lett. 67B, 151 (1977).

[b] A. Dudek-Ellis, V. Shkolnik, J. L. Artz, D. Dehnhard, P. J. Ellis, and H. P. Morsch, Phys. Rev. C 18, 158 (1978).

gated in the same way to generate the corresponding spectra. Specific mass groups could not be adequately resolved in these Z groups.

To arrive at relative direct reaction strengths for the various ejectiles, the yield over the first 10 MeV excitation in each ejectile spectrum was integrated for $\theta_{lab}=14.7°$, 18°, and 21°. The energy calibration necessary for this analysis was generated from known discrete peaks in the various ejectile spectra at the different angles. It was assumed that the N, O, and F reaction products were ^{15}N, ^{16}O, and ^{19}F for energy calibration purposes. The results are unchanged if it is assumed the groups are ^{14}N, ^{18}O, and ^{18}F. As discussed previously, the contribution from the Formvar backing was subtracted from the ^{27}Al + Formvar spectra. The contribution due to the oxygen in the $^{28}SiO_2$ targets was similarly subtracted from the ejectile spectra by obtaining the oxygen yield from the $^{27}Al_2O_3$ + Formvar and ^{27}Al + Formvar data.

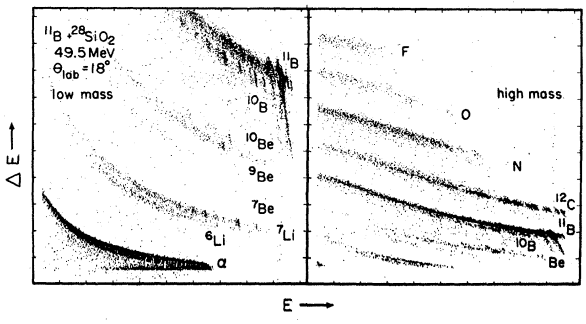

FIG. 8. Multiparameter E-ΔE spectra of 49.5 MeV ^{11}B+$^{28}SiO_2$ taken at $\theta_{lab}=18°$. Particle groups are identified from $3 \leq Z \leq 9$.

Figure 9 shows the comparison of the ^{11}B + ^{27}Al and ^{11}B + ^{28}Si direct reaction product strengths. Lab cross sections were computed at each angle by normalizing the yields to the known elastic scattering cross ection. Those cross sections were multiplied by $2\pi \sin\theta$ and summed over the three angles. These are plotted in Fig. 9.

The single particle transfer reaction products ^{10}B and ^{12}C are 2 and 4 times stronger in the ^{11}B + ^{28}Si system than in the ^{11}B + ^{27}Al system. In the other exit channels, ^{11}B + ^{28}Si is also largest. However, these other channels are at least an order of magnitude smaller than the ^{28}Si(^{11}B, ^{10}B) and ^{28}Si(^{11}B, ^{12}C) reaction strengths.

IV. DISCUSSION

Data have been presented which show similarities in the elastic scattering angular distributions of ^{10,11}B + ^{27}Al, ^{28,30}Si from 34 to 50 MeV, except in the case of ^{11}B + ^{28}Si. Optical model parameters were obtained for each case. The ^{10}B potentials exhibit slightly varying degrees of absorption, but the differences are not significant. The optical model analysis of the ^{11}B + ^{28}Si showed ^{11}B + ^{28}Si to be more strongly absorbing than the other systems.

Inelastic scattering data for ^{10,11}B + ^{28,30}Si are also presented. Significant differences in inelastic scattering cross sections between ^{10}B + ^{28}Si and ^{11}B + ^{28}Si were sought as explanations for the elastic scattering differences. However, the data presented for these cases are similar in both

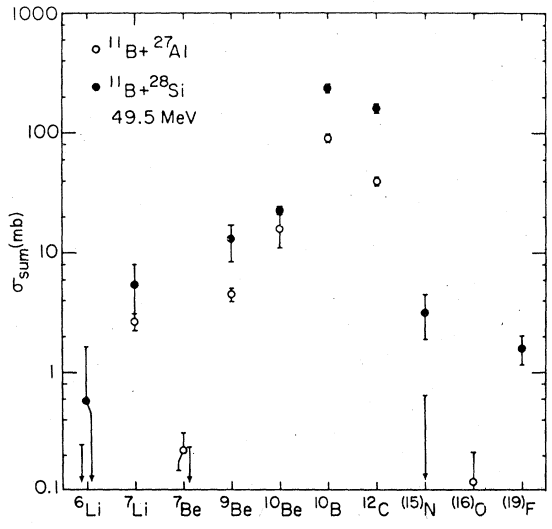

FIG. 9. A comparison of relative strengths of ^{11}B+^{27}Al and ^{11}B+^{28}Si direct transfer reactions. The lab cross sections at 14.7°, 18°, and 21° were multiplied by $2\pi \sin\theta$ and summed over the three angles to produce σ_{sum}. In the treatment of the data, it is assumed that the N, O, and F groups were ^{15}N, ^{16}O, and ^{19}F.

magnitude and shape. The $^{10,11}B + ^{28}Si$ inelastic angular distributions both show similar oscillatory structure as opposed to obvious dissimilarities when comparing the elastic scattering angular distributions. Additionally, the β_N^2 used to normalize the calculations to the 49.5 MeV data indicate that the 2^+ state in ^{28}Si is populated with the same strength by both ^{10}B and ^{11}B projectiles.

The reaction data offer an explanation for the differences seen about the grazing angles in the $^{11}B + ^{28}Si$ elastic scattering compared to the $^{10,11}B + ^{27}Al$, ^{30}Si and $^{10}B + ^{28}Si$ elastic scattering. Comparison of the direct reaction strengths of the ejectiles from 49.5 MeV $^{11}B + ^{27}Al$ and $^{11}B + ^{28}Si$ show that the $^{28}Si(^{11}B, ^{12}C)^{27}Al$ direct reaction strength is ~4 times larger than that for $^{27}Al(^{11}B, ^{12}C)^{26}Mg$. Additionally, the $^{28}Si(^{11}B, ^{10}B)^{29}Si$ direct reaction strength is ~2 times larger than the $^{27}Al(^{11}B, ^{10}B)^{28}Al$ direct reaction strength. Therefore, at least 2 direct reaction channels are significantly stronger in the case of $^{11}B + ^{28}Si$ than for $^{11}B + ^{27}Al$. These stronger reaction channels may be the cause of the $^{11}B + ^{28}Si$ elastic scattering differences.

The present work shows, as was also shown by Henning *et al.*,[10] that it is necessary to include the transfer reaction channels in coupled channels calculations, before a detailed understanding of direct heavy-ion transfer reactions can be possible.

The authors would like to thank L.Courtney and C. Glover for their aid in obtaining the experimental data and R. Leonard for fabrication of the targets. Conversations with F. Petrovich, D. Robson, and D. Stanley are also gratefully acknowledged. This work was supported in part by the National Science Foundation.

---

*Present address: IRT Corporation, San Diego, California 92138.

†Present address: Cyclotron Laboratory, Department of Physics, Michigan State University, East Lansing, Michigan 48824.

[1]L. A. Parks, K. W. Kemper, A. H. Lumpkin, R. I. Cutler, L. H. Harwood, D. Stanley, P. Nagel, and F. Petrovich, Phys. Lett. 70B, 27 (1977).

[2]K. R. Chapman, Nucl. Instrum. Methods 124, 229 (1975).

[3]F. G. Perey, Phys. Rev. 131, 745 (1963); A. W. Obst, Florida State University Technical Report No. JIB, 1973 (unpublished).

[4]J. S. Blair, Phys. Rev. 115, 928 (1959).

[5]G. Igo, Phys. Rev. Lett. 1, 72 (1958); Phys. Rev. 115, 1665 (1959).

[6]P. J. Moffa, C. B. Dover, and J. P. Vary, Phys. Rev. C 13, 147 (1976).

[7]G. R. Satchler, in *Proceedings of the International Conference on Reactions Between Complex Nuclei*, edited by R. L. Robinson, F. K. McGowan, J. B. Ball, and J. H. Hamilton (North-Holland, Amsterdam, 1974), Vol. 2, p. 171.

[8]J. G. Cramer, R. M. DeVries, D. A. Goldberg, M. S. Zisman, and C. F. Maguire, Phys. Rev. C 14, 2158 (1976).

[9]P. D. Kunz, University of Colorado, private communication.

[10]W. Henning, J. P. Schiffer, D. G. Kovar, S. Vigdor, B. Zeidman, Y. Eisen, and H. J. Körner, Phys. Lett. 58B, 129 (1975).